

Energetic Ion Production and Electrode Erosion in Hollow Cathode Discharges

IEPC-2005-266

*Presented at the 29th International Electric Propulsion Conference, Princeton University,
October 31 – November 4, 2005*

Dan M. Goebel^{*}, Kristina Jameson[†], Ira Katz[‡], Ioannis G. Mikellides[§]
Jet Propulsion Laboratory, California Institute of Technology, Pasadena, CA 91109

Abstract: Ions with energies significantly in excess of the discharge voltage have been reported in high current hollow cathode discharges. Models of DC potential hills downstream of the cathode and ion acoustic instabilities in a double layer postulated in the cathode orifice have been proposed to explain these energetic ions, but have not been substantiated by experiments. An investigation of the DC and rf density and potential profiles measured throughout the discharge by fast miniature scanning probes suggests that turbulent oscillations in the characteristic “plasma ball” observed downstream of the cathode orifice are responsible for both the energy and spatial distribution of the energetic ions. Keeper erosion rates and wear profiles are discussed with respect to the production and trajectories of these high energy ions.

I. Introduction

Hollow cathodes have been used in a multitude of applications to produce plasma for ion sources, lasers, plasma processing, etc. The primary purpose of enclosing the electron emitter inside a hollow structure and extracting electrons from the cathode plasma through an orifice is to protect the thermionic emitter from energetic ion bombardment that can degrade the work function of the surface¹. The hollow cathode is also often enclosed inside another electrode called the keeper that is a biased hollow tube with a slightly larger orifice aligned with the cathode aperture. The purpose of the keeper is to draw a small amount of current from the cathode to facilitate turn-ON, to maintain the cathode temperature if the main discharge current is turned off or interrupted, and to protect the cathode orifice plate from ion bombardment and erosion.

With sufficient gas flow, orificed thermionic hollow cathodes can produce quiescent discharges at modest currents of ten’s of amperes. However, as the discharge current is increased, the noise observed in the discharge voltage and probe signals from the plasma increases, and the cathodes produce ions with energies significantly in excess of the discharge voltage²⁻⁶. Cathode orifice plate and keeper electrode erosion rates measured or inferred in various experiments^{7,8} and in ion thruster life tests^{9,10} have been found to be much higher than anticipated. These results have been attributed to the high-energy ions bombarding and sputtering the cathode electrodes. Of particular concern is the apparent change in the erosion pattern at different discharge power levels in the NSTAR ion thruster^{11,12} Extended Life Test (ELT)¹⁰ that caused the keeper to entirely erode away in less than 15,000 hours. The source and characteristics of these high-energy ions has been a subject of much research and debate. Models of a DC potential hill¹³ located inside or just downstream of the cathode orifice, or ion acoustic instabilities in a double layer postulated in the orifice of the cathode², have been proposed to explain the production of these ions. However,

^{*} Principal Scientist, Jet Propulsion Laboratory, dan.m.goebel@jpl.nasa.gov

[†] Graduate Student, University of California, Los Angeles, kristina.k.jameson@jpl.nasa.gov

[‡] Group Supervisor, Advanced Propulsion Group, Jet Propulsion Laboratory, ira.katz@jpl.nasa.gov

[§] Senior Engineer, Jet Propulsion Laboratory, Ioannis.G.Mikellides@jpl.nasa.gov

there have been no direct measurements in probe studies to date^{15,16} of potential hills or unstable double layers at the cathode orifice or in the cathode plume that might explain the mechanisms responsible for the high-energy ions or the electrode wear rates and patterns.

To investigate this issue, the hollow cathode test facility at JPL was instrumented with an array of scanning probes and a 4-grid retarding potential analyzer (RPA). The probes are very small (0.5-mm-dia. ceramic tubes) to avoid perturbing the plasma, and are scanned pneumatically at speeds of up to 2 m/sec to avoid melting in the high density plasmas. A standard 1/4" NSTAR cathode was installed in a conical-to-cylindrical anode that approximates the NSTAR ion thruster geometry and operated at various throttle levels. In addition, a 1.5-cm diameter NEXIS hollow cathode was also installed in the facility and tested to determine the effect of cathode size and current scaling on the keeper erosion physics.

The experiments detected a significant amount of high energy ions traveling in the radial direction from the characteristic plasma ball observed in front of the cathode. The high speed scanning rf probes capable of measuring the rf plasma potential detect significant plasma oscillations in the ion acoustic range from the edge of the plasma ball near the cathode. A detailed investigation of the DC and rf density and potential profiles measured throughout the hollow cathode discharge by the scanning probes indicates that there is no DC potential hill at or near the cathode orifice. In the orifice, a potential discontinuity or double layer with a magnitude of less than 10 V has been detected that has ion-acoustic type oscillations on the order of 1 MHz, but these are small in amplitude ($\Delta n/n \approx 1\%$). Outside the keeper, the plasma potential forms a well or trough centered on the high density "plasma ball" observed there, with the potential increasing axially over several cm to a peak value near the discharge voltage and radially to potentials 5 to 10 V in excess of the discharge voltage that extend to near the anode surface. Measurements of the plasma potential fluctuations with a high impedance emissive probe constructed to be sensitive to up to 1 MHz show large amplitude fluctuations (> 50 V) in the plasma potential ranging from 70 to 500 kHz starting at the edge of the ball and extending radially outward to the wall. The collected RPA current is related to the density and potential fluctuations measured by the probes. The plasma potential fluctuation are found to be small in the axial direction, and do not extend into the cathode. In the radial direction, the potential fluctuations can exceed five times T_e , suggesting turbulent acoustic oscillations near the edge of the "plasma ball" are responsible for both the high energy and spatial distribution of the energetic ions. The axial location of the plasma ball is observed to change with the throttle level, with the NSTAR TH8 setting pulling the ball back into the keeper orifice. This may explain the rapid radial erosion of the keeper observed at this setting due to the primarily radially directed high-energy ions directly bombarding the keeper orifice inside diameter. The RPA and probe measurements will be presented for the two cathodes with discussion of the impact on keeper erosion.

II. Experimental Arrangement

The JPL hollow cathode test facility¹⁵ was instrumented with an array of scanning probes and a 4-grid retarding potential analyzer (RPA), as illustrated in Fig. 1. Two hollow cathodes were investigated in these experiments. The first is a conventional NSTAR-size cathode¹ with a 6.35-mm diameter molybdenum-rhenium tube with a 1-mm diameter orifice. A porous tungsten emitter impregnated with a low-work-function barium-calcium-aluminate mixture is located inside the cathode. Electrons emitted from the insert by field-enhanced thermionic emission generate a cathode plasma inside the insert region, from which electrons are extracted through the orifice to generate the plasma in the discharge chamber. The cathode is heated by a standard sheathed heater, which is turned off during discharge operation. A keeper electrode made from molybdenum or graphite fully encloses the cathode, and the keeper orifice is about 4.6 times the diameter of the cathode orifice. The second cathode is a conventional barium impregnated tungsten insert in a 1.5 cm dia. molybdenum tube with a tungsten orifice plate e-beam welded on the end. The cathode is heated by a standard sheathed heater, which is turned off during discharge operation. The NEXIS graphite keeper electrode also fully encloses the cathode, and the keeper orifice is about 1.7 times the diameter of the cathode orifice.

The cathode and scanning probe system are mounted on an 8" Conflat flange installed in one port of 0.75-m diameter, 2-m long vacuum chamber. The chamber is pumped by two 10" CTI cryopumps with a combined xenon pumping speed of 1275 l/sec for xenon. The base pressure of the chamber is in the 1×10^{-8} Torr range, and during normal operation at less than 5 sccm of xenon flow the chamber pressure remains in the low 10^{-5} Torr range, where the xenon gas is controlled and measured by a digital MKS mass flow controller. Additionally, a precision Baratron capacitive manometer is used to measure the pressure in the hollow cathode during operation.

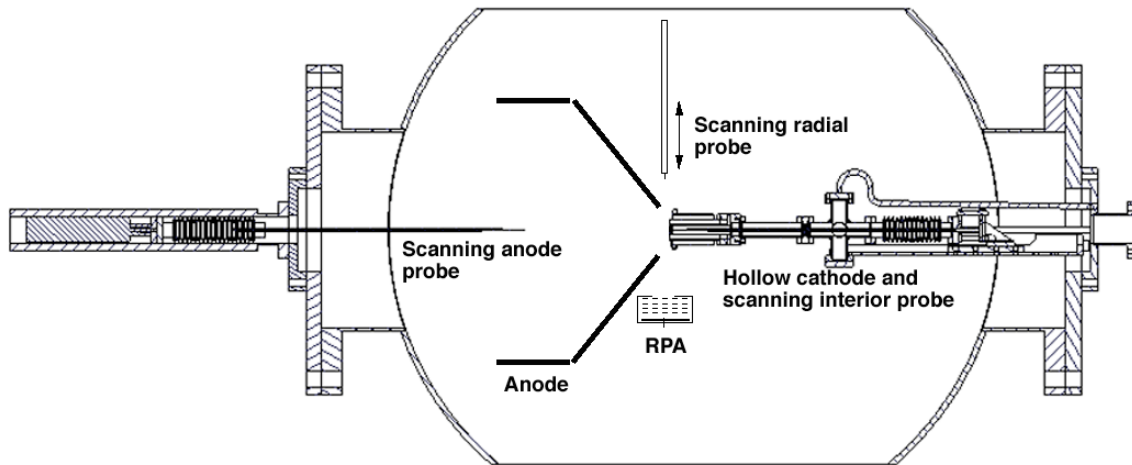


Figure 1. Schematic drawing of the experimental layout showing the cathode, anode, three scanning probe diagnostics and the retarding-potential analyzer (RPA) which could be located radially (shown) or axially from the cathode.

The cathode scanning probe assembly mounted in the vacuum system is shown in Figure 2a. The experimental arrangement uses a water-cooled anode that has a conical section and a cylindrical section approximately 30 cm in diameter with an NSTAR-like magnetic field arrangement. The probe tip is 0.5 mm diameter alumina tubing with a 0.127 mm diameter tungsten wire electrode that protrudes from the small-bore ceramic tubing a distance of 0.25 mm. Even though the wire electrode is kept at a minimal length for electron collection, the probe has collected up to 5 A of current in the high density region near the orifice of the cathode. The cathode probe is aligned axially in the system by two slide-guides internal to the cathode system. The probe has a linear throw of 4 cm and can traverse the cathode at one meter per second with a resolution of 0.25 mm. A dual bellows system in the cathode assembly is used to keep constant volume inside the cathode assembly, which maintains a constant pressure in the cathode while the Langmuir probe is being inserted into and out of the insert region. The cathode probe occupies about 30% of the cathode orifice cross sectional area, and does significantly perturb the plasma discharge if the probe is pushed too far past the upstream orifice entrance. For this reason, data is only taken prior to the probe entering the cathode orifice. Also shown in Fig. 2a is a solenoid coil wound on a water cooled cylinder directly around the cathode to provide a diverging axial magnetic field of adjustable amplitude at the cathode exit that simulates the cathode field in ring-cusp thrusters. See reference 7 for a full description of the cathode probe assembly.

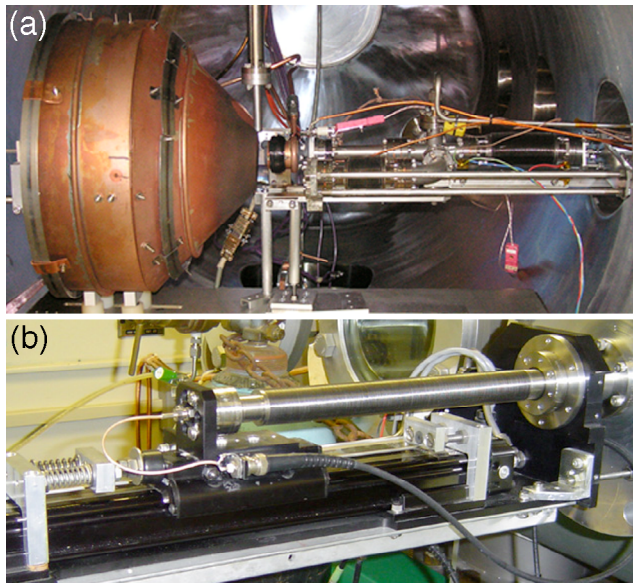


Figure 2. Scanning probe assemblies (a) cathode probe mounted in the vacuum chamber with the conical-to-cylindrical water cooled anode with ring-cusp magnets, and (b) the anode probe drive system outside the vacuum system showing the high speed pneumatic plunger and bellows arrangement.

The anode scanning-probe assembly is shown in Figure 2b, where the pneumatic plunger and vacuum bellows arrangement mounted on the outside of the vacuum system are seen. The diameter of the ceramic tubing interior to the vacuum system is stepped down from 3 mm to 0.5 mm diameter for the 3cm section that is inserted deepest into the plasma in order to

minimize perturbation to the plasma in the anode region. The exposed electrode is again a 0.127 mm tungsten wire, but has a length of 1.3 mm to collect sufficient current away from the keeper region to accurately determine the plasma parameters. The anode probe has nearly three times the throw of the cathode probe and 5 times the unsupported length so as to not perturb the anode-plasma, and also moves at one meter a second with a position resolution of 0.5 mm. Very careful iterative alignment techniques are used to ensure that the anode probe is aligned with the cathode orifice and within 0.5 mm of the centerline. The anode probe can be fully inserted into the keeper orifice, although whip of the long ceramic sometimes causes the tip to touch the keeper or cathode during retraction.

A radially scanning emissive probe is seen in Figure 3. It uses a pneumatic plunger, identical to the cathode plunger, and is mounted to a Huntington X-Y manipulator outside the vacuum system to provide positioning relative to the keeper exit point. The radial probe has a linear throw of 3 cm, also at one meter per second, and is aligned by a slide-guide internal to the vacuum system to obtain a position resolution of 0.25 mm. The probe can be positioned in front of the keeper as close as 1 mm out to 2.5 cm downstream. The probe tip is a 0.127 mm diameter tungsten hair-pin wire feed through two side-by-side 0.5 mm diameter alumina tubes. A floating 5 amp power supply provides the current to heat the tungsten wire electrode to emit electrons. The probe signal fed to a high impedance, high frequency circuit and a buffer amplifier to detect any oscillations present in the signal. When the emissive probe is not in use, it resides in 6.5-mm-dia. tube that is positioned sufficiently out of the discharge plume to protect it from ion bombardment.

A gridded retarding potential analyzer is used to determine the ion energy distribution. A four-grid arrangement was used where the first grid in contact with the plasma floats, the second grid is biased to repel electrons, and only the ions with energy greater than potential applied to the dual-discriminator grid can pass through and reach the collector. Figure 1 shows the RPA only positioned radially in the gap between the anode and the keeper, which is shown in the photograph of the experimental arrangement in Fig. 4. However, the RPA could also be placed on axis to obtain axial energy distributions downstream from the cathode. In this case, the anode probe assembly is removed from the chamber to allow the RPA to be placed unobstructed on axis at the exit of the anode.

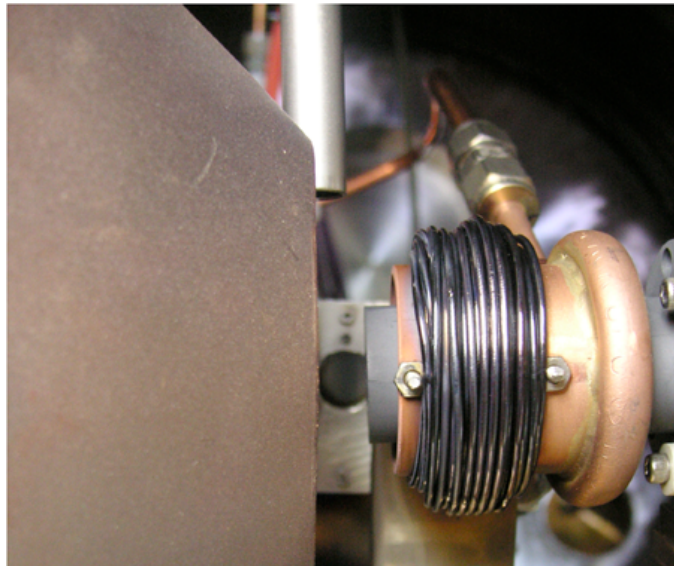


Figure 4. Photograph of the NSTAR cathode, conical anode, RPA in the background, and transverse probe coming in from the top.

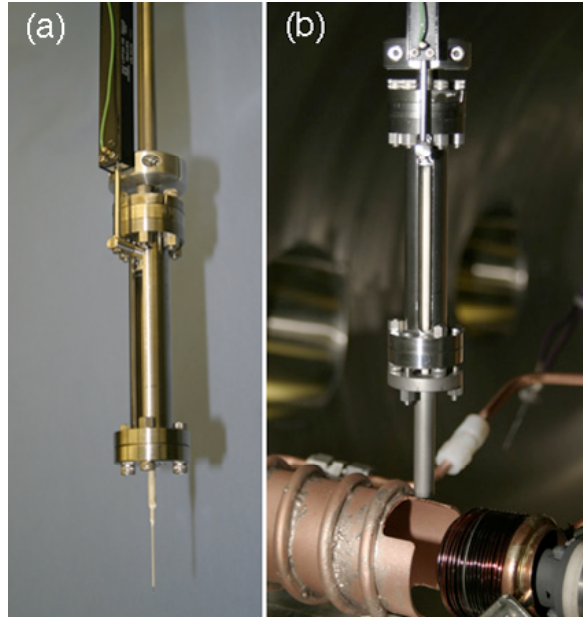


Figure 3. Transverse scanning probe with position transducer (a), and being tested with NSTAR cathode and small cylindrical anode (b).

Experiments are conducted with a NSTAR like anode with a diverging conical section followed by a straight cylindrical section, constructed of copper and water cooled. The anode can be seen in Fig. 2a and the entrance where the cathode was placed is seen well in Fig. 4. The conical section has a minimum diameter of approximately 5 cm, and is joined to the 30-cm-dia. straight cylindrical section. The gap between the cathode keeper exit and anode is adjustable, and is typically about 2 cm to allow for visualization of the cathode plume and

to acquire radial RPA traces. A solenoid coil positioned around the cathode produces an axial magnetic field at the cathode orifice, which couples to two rings of permanent magnets around the anode body to simulate the NSTAR magnetic field geometry. This anode geometry is capable of reproducing the full NSTAR throttle table, producing discharges at 6.1 A at 26.8 V representing TH4, 8.2 A at 26 V representing TH8, 10.9 V at 26.2 V representing TH12, and 13.1 A and 25.2 V representing TH15.

The bias voltage applied to the probe tips is generated by a programmable waveform synthesizer that drives a Kepco bipolar power supply. The voltage waveform is a sawtooth ramp that scans from -10 to + 50 V in the anode region and from -10 to +20 in the cathode region in a time of 1 msec. When using the NSTAR cathode, the cathode probe can only be swept once per insertion to avoid overheating the probe tip in the very high-density plasma ($>10^{15}$ cm⁻³ density) near the hollow cathode orifice. A delay generator is used to take consecutive traces allowing the cathode plasma parameters can be mapped. The NEXIS cathodes has nearly an order of magnitude lower pressure inside and corresponding lower plasma density, so that multiple voltage sweeps can be made during the probe insertion to map-out the plasma profiles with a single scan. Electron temperatures and plasma potentials are determined in less than half of the total 1 msec trace, therefore the position uncertainty for the plasma parameters is on the order of 0.5 mm over most of the scan and less than 0.25 mm near the full insertion point. The probe position, voltage and current data is collected on a PC at a sample rate of 300 kHz, resulting in 300 data points in each probe characteristic curve. The plasma potential and electron temperatures are found by classical Langmuir probe analysis. The electron temperature is found by fitting an exponential curve to the electron retardation region of the Langmuir trace. The electron temperatures have error bars about ± 0.5 V and the plasma potentials have error bars of ± 1 V in the cathode region and up to ± 2 V in the anode region.

III. NSTAR Cathode Results

The NSTAR thruster is normally operated over a variety of parameters described in a “throttle table”, which is designed to keep the discharge voltage at about 25 V while the gas flow rate and/or the discharge current is changed to produce different thrust levels.⁶ In these experiments, we operated primarily at four throttle conditions (TH4, 8, 12 and 15), with the majority of time investigating the performance in TH15 and TH8 where the keeper erosion data is extensive. The keeper erosion in the NSTAR thruster represents a significant potential failure mechanism. Figure 5 shows a cross section of the keeper electrode after the 8200 hour Long Duration Test (LDT) at JPL. In this test, the thruster was operated at the highest power level, TH15, corresponding to 2.3 kW of total thruster power and a discharge current of 13 A at about 25 V. The molybdenum keeper downstream face was significantly eroded during the test. Figure 6 shows

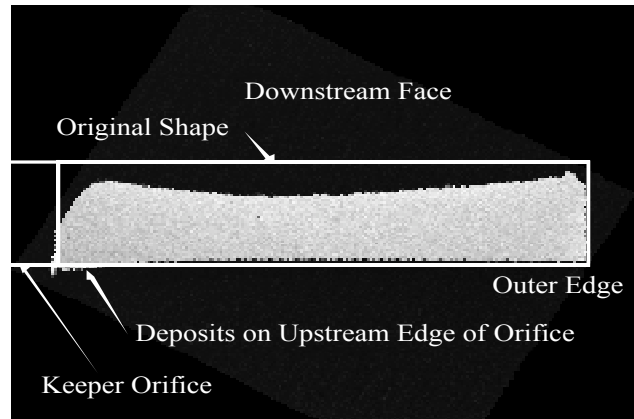


Figure 5. NSTAR keeper cross section after the 8200 hour LDT test at TH15 showing significant erosion of the keeper face.



Figure 6. Photo of the NSTAR cathode at the start of the ELT test and after 30,352 hours where the keeper electrode completely eroded away.

photographs of the NSTAR cathode assembly at the start and conclusion of the ELT test, illustrating the complete sputter erosion removal of the keeper electrode. The face of a graphite keeper on the NSTAR cathode that was run in the test facility for less than 20 hours is shown in Figure 7. While there is no significant erosion of the graphite because its sputtering yield is significantly lower than molybdenum, the surface discolorization shows the ion bombardment in the same region radially away from the cathode orifice. However, sequential photographs of the keeper electrode during the ELT test showed that the keeper eroded significantly faster

during operation at the TH8 throttle level. The reason for this high erosion in the lower power TH8 throttle mode has not been explained.

To try and understand the keeper erosion mechanism, we measured complete axial and radial profiles of the plasma density, potential and electron temperature in the cathode and keeper regions. The plasma density inside the NSTAR cathode is very high, and typically exceeds 10^{15} cm^{-3} for all but the lowest throttle points. In changing operating conditions from TH8 to TH15, which increases in both discharge current and flow rate, the density profile is shifted downstream toward the orifice and is steeper, shown in Figure 8. The neutral pressure inside the cathode for TH15 is on the order of 8 to 9 Torr, and is about 1.7 times that of TH8. Higher neutral pressures in the insert region are observed to cause the cathode plasma density to fall more rapidly upstream from the orifice, and reduce the already small contact length to. The plasma is in contact with the insert typically less than about 3 mm for this cathode, suggesting that cathodes with pressures approaching 5 to 10 Torr may only utilize a fraction of the insert length for any significant electron emission.⁷ Surprisingly, the probe signal for the TH8 case is much noisier than that for the TH15 case, which was related to large oscillations external to the cathode, to be discussed later. It appears that the plasma in the cathode and keeper orifice regions for TH08 is inherently less stable than for TH15, probably due to the combination of gas flow and discharge current selected for this mode.

The axial plasma potential and electron temperatures measured through the hollow cathode plasma and into the keeper region are shown in Fig. 9 for the TH15 and TH8 modes. The 13-A TH15 mode shown in Fig.9a has a plasma potential inside the insert of about 6 V, while a higher 8 to 9 V potential is required inside the 8.2A TH8 mode in Fig. 9b to self heat the cathode. The electron temperature in both cases is on the order of 1.5 eV. The potential in the orifice region is difficult for the probes to measure because the probe ceramic cross sectional diameter is only twice the orifice diameter, and the discharge is significantly perturbed by inserting the probe deep into the orifice. However, the probe inserted from the anode side can penetrate inside the keeper orifice with a couple of millimeters of the cathode orifice. We see that the potential has jumped to the order of 12 to 14 V, and then increases slowly as the probes moves away from the keeper orifice. The potential is found to reach the about the anode potential within 10 cm of the cathode.

The plasma density and potential profiles downstream of the keeper electrode in the NSTAR geometry have been extensively measured with scanning probes by Herman and Gallimore, Jameson, et al., and by Sengupta, et al., and their results are consistent with our data when our probes are configured to measure the time-averaged plasma parameters. An example of the radial plasma potential profile measured by our scanning emissive probe about 2 mm downstream of the keeper for TH15 is shown in Figure 10. In this case, the data acquisition system is averaging the data at about 1 kHz, so this data represents the average radial potential profile. We see that the plasma potential is about 12 V on axis, in agreement with the anode probe data in Fig. 9a. The potential is a minimum on axis and increases to above the anode potential a distance of about 1 cm from



Figure 7. Graphite keeper face discoloration showing ion bombardment pattern for approximately 20 hours of operation at TH15.

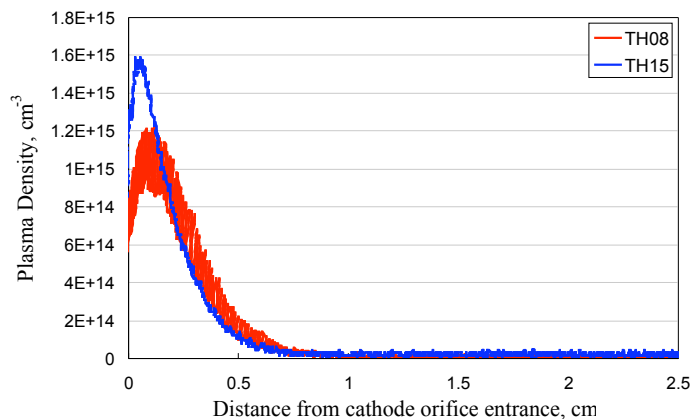


Figure 8. Cathode density profiles plotted on a linear scale for TH8 and TH15.

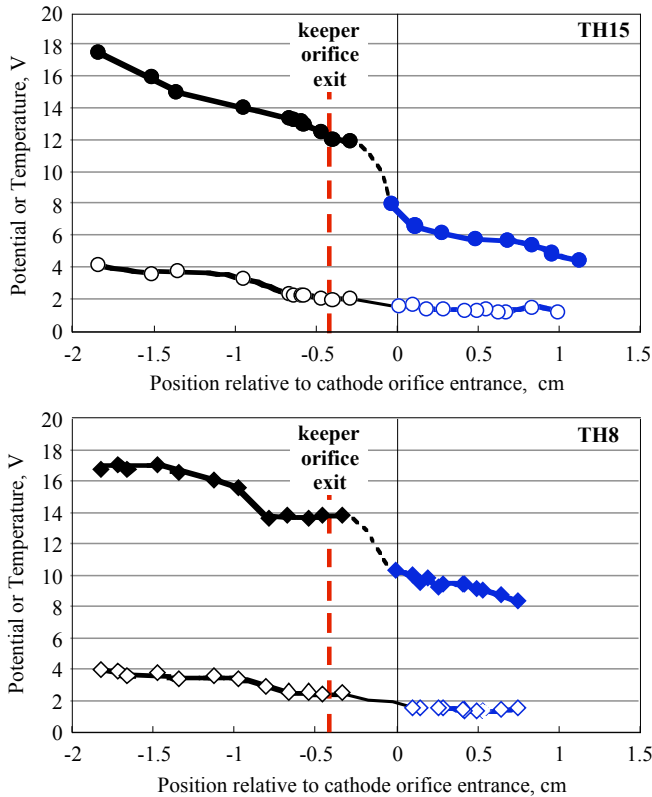


Figure 9. Plasma potential and electron temperature for the cathode-keeper region for TH15 (a) and TH8 (b).

potential above the anode voltage as shown in Fig. 10. However, the radial ion energy distribution shows there a large number of ions with energy significantly higher than the discharge voltage and extending out beyond 100 V. These ions certainly have sufficient energy to cause keeper erosion, and are produced in the region just downstream of the keeper electrode where the radial analyzer is collecting.

The ion energy distribution functions in the axial and radial directions for the TH8 throttle point are shown in Fig. 12. The axial distribution shows the typical peak at about the discharge voltage, and essentially no ions with energy in excess of 40 volts. The ion energy is a result of the ions falling from the potential at which they were created into the cathode-potential analyzer. An analysis of the sputtering rate of the cathode and keeper orifices indicates that ions with nearly twice this energy would be required to produce the observed erosion rates in the ion thruster tests⁸⁻¹⁰. The radial ion distribution, on the other hand, shows a significant number of ions at energies above the peak near the anode voltage.

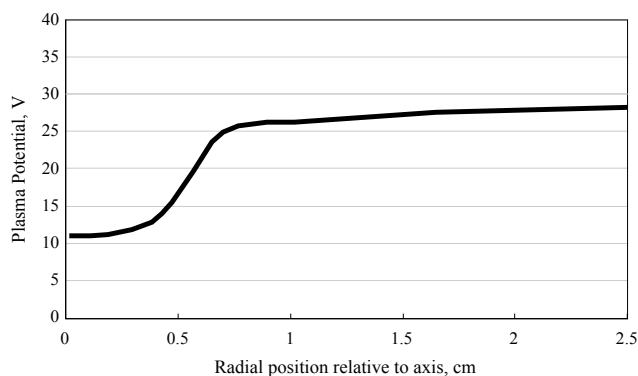


Figure 10. Time averaged radial profile of the plasma potential for TH15 operation from an emissive probe.

the axis. Similar profiles extend axially such that the cathode plume forms a potential trough, with the potential increasing radially and axially from the keeper orifice. This of course is inverse to the plasma density profiles, which are peaked near the orifice and decrease radially and axially away.

To better understand the keeper erosion mechanisms, a retarding potential analyzer (RPA) was placed both on axis and radially in the gap between the keeper and the anode to diagnose the ion energy distributions. The ion energy distributions measured in the axial and radial directions from the RPA in the TH15 mode are shown in Figure 11. The radial measurement is taken directly in front of the keeper electrode, as shown in Fig. 1. The axial distribution has a peak at the discharge voltage, and a larger peak observed at a lower potential. Since the RPA only collects ions falling from the plasma potential peak, there are many ions born on the downward slope between the axial potential peak at the discharge voltage and the analyzer that fall into the analyzer. Significantly, there are essentially no ions with energies in excess of 35 V measured on axis. The ion distribution function measured in the radial direction has a peak slightly above the anode voltage, corresponding to ions born off axis at the

potential above the anode voltage as shown in Fig. 10. However, the radial ion energy distribution shows there a large number of ions with energy significantly higher than the discharge voltage and extending out beyond 100 V. These ions certainly have sufficient energy to cause keeper erosion, and are produced in the region just downstream of the keeper electrode where the radial analyzer is collecting.

The ion energy distribution functions in the axial and radial directions for the TH8 throttle point are shown in Fig. 12. The axial distribution shows the typical peak at about the discharge voltage, and essentially no ions with energy in excess of 40 volts. The ion energy is a result of the ions falling from the potential at which they were created into the cathode-potential analyzer. An analysis of the sputtering rate of the cathode and keeper orifices indicates that ions with nearly twice this energy would be required to produce the observed erosion rates in the ion thruster tests⁸⁻¹⁰. The radial ion distribution, on the other hand, shows a significant number of ions at energies above the peak near the anode voltage.

A direct comparison of the two radial ion energy distributions for TH8 and TH15 is shown in Figure 13. The number of ions in the peak just above the anode voltage is larger for the TH15 case because the plasma density is about twice as high in TH15 compared to the TH8 case. However, the TH8 case appears to have a comparable number of high energy ions, which is remarkable since the density is half of the TH15 case. The comparable number of high-energy ions in the two cases suggest that the keeper erosion in the ELT tests in the TH8 mode should have been comparable to the TH15 mode. This was not observed, and so an alternative mechanism must be pursued associated with the fact that the TH15 erosion was largely to the keeper face (axial) and

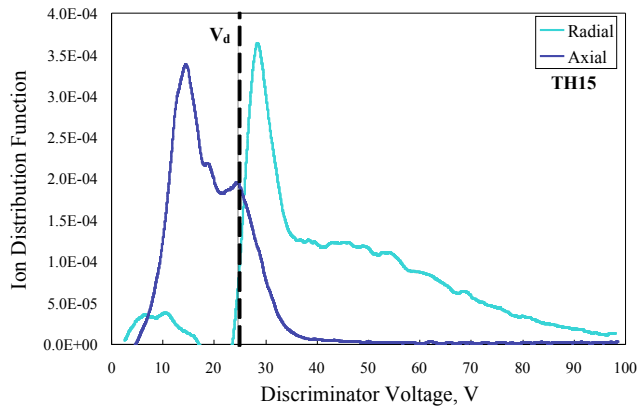


Figure 11. Ion energy distributions for TH15 both radially and axially.

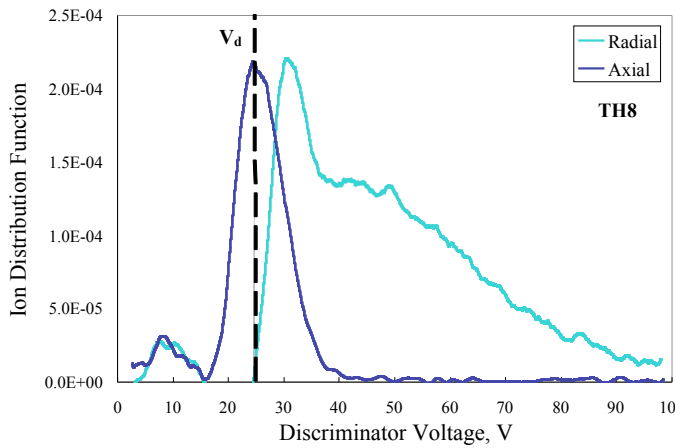


Figure 12. Ion energy distributions for TH8 both radially and axially.

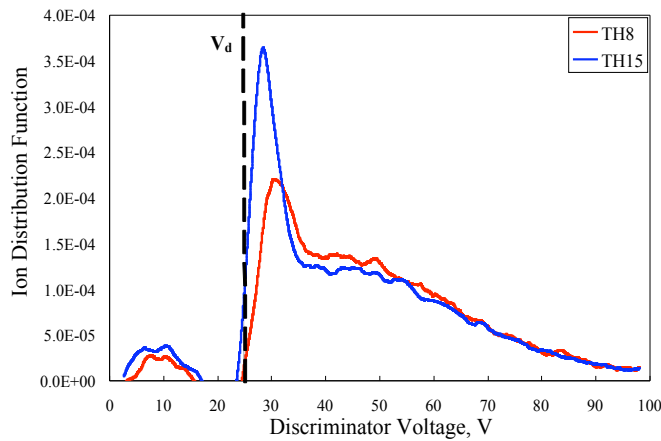


Figure 13. Comparison of radial ion energy distributions for TH8 and TH15.

the TH8 erosion was largely radial. The axial erosion can be mitigated by manufacturing the keeper face plate out of a different material with a lower sputtering yield and by making the plate thicker, hence tantalum and graphite keepers have been suggested for future missions using the NSTAR thrusters.¹⁰

The source of the high-energy ions flowing in the radial direction for both throttle levels is of interest. Since the ions fall from the potential at which they are created, there is no mechanism for the observed high ion energy in the DC-averaged potential profiles we measured and that are found in the literature. However, if the plasma potential is oscillating, the ions can be created at a higher potential and gain sufficient energy falling to the keeper voltage to sputter the keeper at high rates. The rf oscillations of the plasma potential in the cathode plume were examined with the transverse emissive probe operated in the emission limited mode. In this case, the probe filament is heated to a sufficient temperature to emit electrons at the random electron flux (or higher), and the probe will float at the local plasma potential. A high impedance circuit ($>10^8 \Omega$) capable of detecting up to 1 MHz oscillations was used to measure the plasma potential fluctuation profile radially in front of the keeper face plate.

Figure 14 shows the radial profile of the plasma potential from the rf-emissive probe at a distance of 2 mm downstream of the keeper for TH15. The white line in the figure is the average plasma potential for the fluctuations in the radial scan. The figure shows again that the average plasma potential is a minimum on axis at 12-14 V, in agreement with the data acquisition averaged Fig. 8. As the emissive probe moves radially outward, the plasma potential increases significantly, and then eventually decreases back to the anode potential near the anode wall. The potential oscillations shown were found to be between 50-500 kHz, depending on the operating conditions. The potential fluctuations range from ± 5 to ± 20 V, with the largest fluctuations starting at about 6 mm from the axis out to 10 mm. Since the fluctuation level approaches 5 to 10 times the local electron temperature, these oscillations are likely turbulent ion acoustic waves. The high frequency fluctuations are observed all along the radial scan, but tend to die out axially and are not observed beyond 5-to-10 cm downstream of

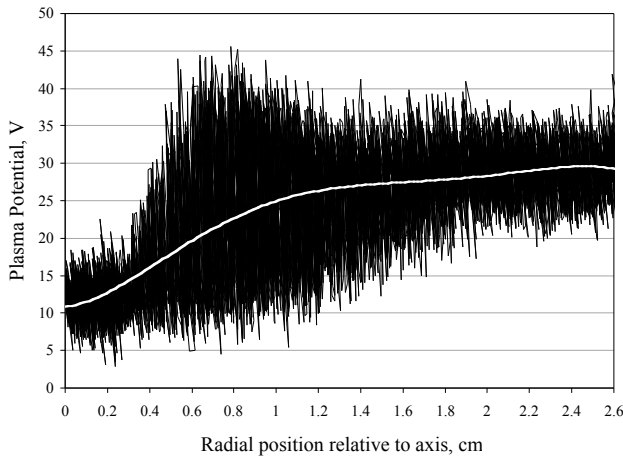


Figure 14. Radial fluctuations in the plasma potential with an emissive probe for TH8.

oscillations are observed to start at the edge of the ball, as seen in Fig. 14. As the discharge is operated at lower throttle levels, the plasma-ball is observed in Fig. 15 to be pulled back into the keeper. During the TH8 mode of interest, the ball is partially inside the keeper and just tail end of the ball can be seen at the downstream end of the keeper orifice, as seen in Figure 15(c). This suggests that the rapid radial keeper erosion observed during TH8 is a result of radially accelerated high energy ions from turbulent ion acoustic waves at the edge of the plasma ball. In the TH15 mode, the plasma ball is significantly outside of the keeper orifice and the majority of these radially-accelerated ions miss the keeper. Ions born in the TH15 mode several millimeters off axis in the large fluctuation region can backstream to the keeper, resulting in the off-axis erosion ring observed in Fig. 6.

IV. NEXIS Cathode Results

To examine the keeper erosion mechanisms scaling with cathode size and provide a detailed study of the oscillations, a NEXIS 1.5-cm-dia. thermionic hollow cathode with a 0.25-cm-dia. orifice was installed in the system. The magnetic field configuration was identical to the NSTAR case, except that the axial field at the cathode orifice was reduced to about 80 G consistent with the NEXIS thruster operation. Figure 16 shows axial plasma density profile measured through the system at 25 A of discharge and 5.5 sccm xenon flow. We see that the density inside the hollow cathode is in the low 10^{14} cm^{-3} range, and falls from there into the anode region. The transverse plasma density profiles for different axial positions from the keeper exit are shown in Figure 17. As with the NSTAR cathode, the plasma density is the highest on axis and near the cathode, and the cathode plume disperses with axial distance from the keeper.

The typical plasma potential and electron temperature profiles measured by the axially scanning probes are shown in Fig. 18 for the same discharge case. At the standard 1-kHz voltage sweep rate used in these experiments and the 1 m/sec probe-scanning speed, the data points in Fig. 18 have a position resolution of about 0.05 cm. While the data acquisition system samples at a rate of 300 kHz/channel, the frequency

the cathode.

In hollow cathode discharges, there is typically a bright plasma “spot” or “ball” that is present in front of the keeper orifice. A series of photographs of the plasma ball are shown in Figure 15 for several cases from TH4 through TH15. In the TH15 mode, this plasma ball can be clearly seen in Fig. 15(a) and extends from the keeper orifice to about 1 cm downstream into the anode plasma. The plasma ball also has a radial extent of less than 1 cm. The large amplitude

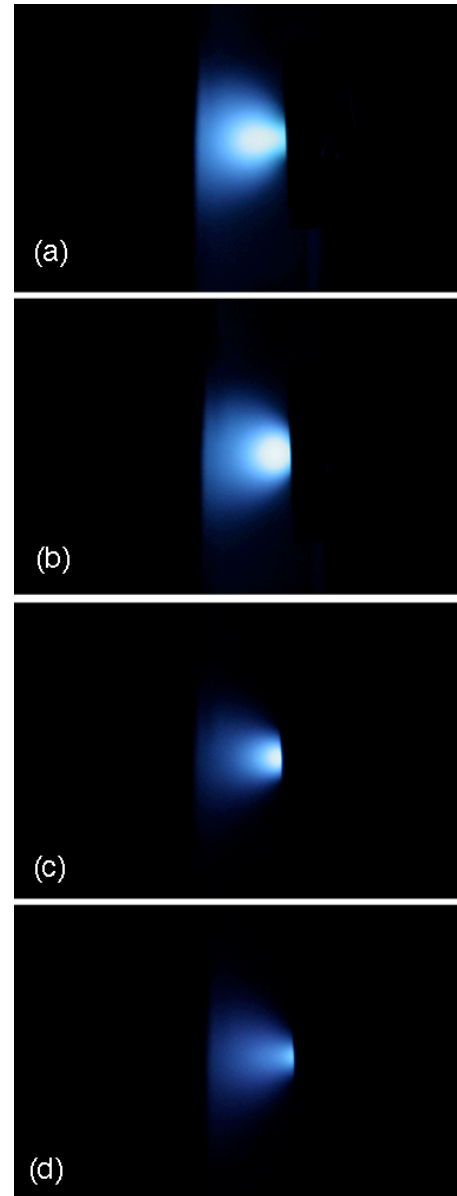


Figure 15. Photos of the plasma ball at the keeper exit for TH15 (a), TH12 (b), TH8 (c), and TH4 (d).

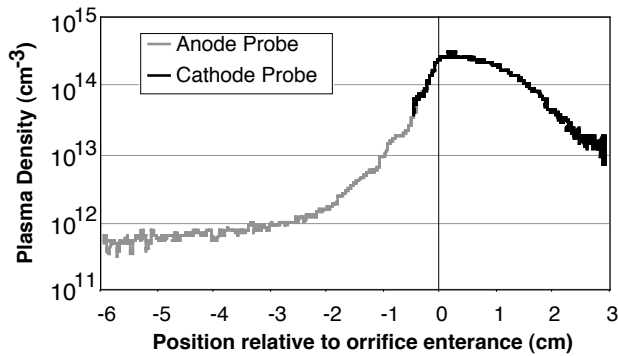


Figure 16. Axial plasma density profile for the NEXIS cathode operating at 25 A and 5.5 sccm gas flow.

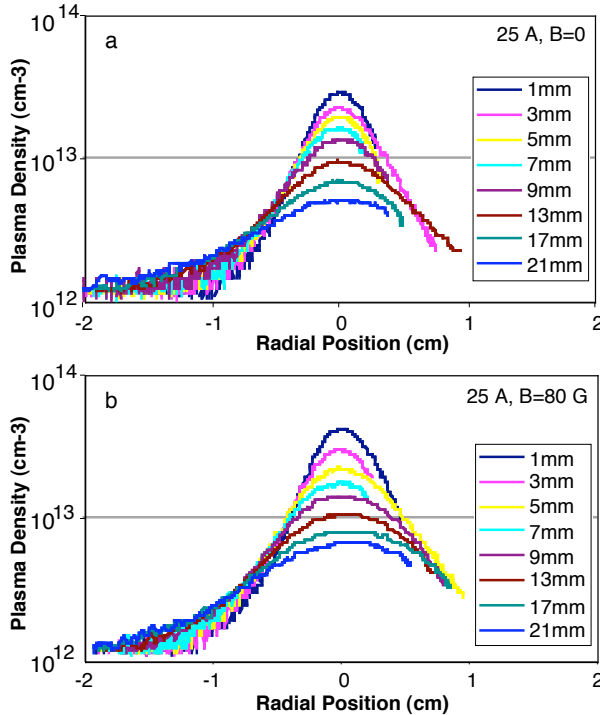


Figure 17. Transverse plasma density profiles.

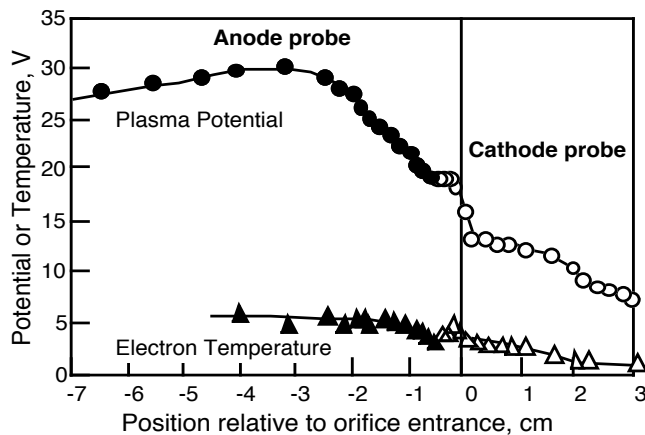


Figure 18. Plasma potential and temperature profiles for the 25 A, 5.5 sccm case.

response of the Langmuir probe circuits is only about 50 kHz.

Inside the hollow cathode, the plasma potential for our nominal discharge conditions is about 12 V above the cathode potential, consistent with obtaining a reduction in the ion energy bombarding the low work-function electron emitting surface. Inside the cathode orifice, a potential discontinuity or double layer with a magnitude of less than 10 V is observed. The plasma potential is essentially flat through the keeper region, and then increases slowly to a peak of about 30 V (about 5 V above the anode potential) several cm downstream of the cathode. The electron temperature is several eV inside the cathode, increasing up to 5 eV in the downstream cathode plume.

Figure 19a shows the ion energy distribution from the axially-oriented RPA for various discharge currents at a constant xenon gas flow with the RPA facing directly at the cathode 25 cm downstream. The RPA discriminator grid was swept at a frequency of 10 Hz during these experiments, so this data represents the time averaged DC ion energy distributions. The ion energy is again a result of the ions falling from the potential at which they were created into the cathode-potential analyzer. The axial data shows a broad distribution of ion energies from ions created at plasma potentials from several eV above cathode potential up to several eV above the discharge voltage. The maximum ion energy measured in this orientation increases slightly with discharge current to on the order of about 40 eV, which is consistent with the ion energies measured on axis in other experiments¹⁷. As mentioned above, ions with nearly twice this energy would be required to produce the observed erosion rates in the ion thruster tests⁸⁻¹⁰.

Figure 19b shows the ion distribution functions for the same discharge cases as in (a) but measured with the RPA positioned immediately downstream of the cathode keeper exit and oriented radially from the cathode plume (as in Fig 1). In this orientation, the RPA detects ions with energies starting at about the discharge voltage and extending to values well in excess of 100 eV. These ions are energetic enough to cause the significant keeper and anode wall erosion from sputtering reported in the literature⁸⁻¹⁰. The high-energy ion tail found in the radial direction from the cathode plume is consistent with measurements at other laboratories of higher energy ions detected in the downstream region of the thruster, but slightly off-axis from the cathode^{3,17}.

As shown in Fig. 18, there is clearly no DC

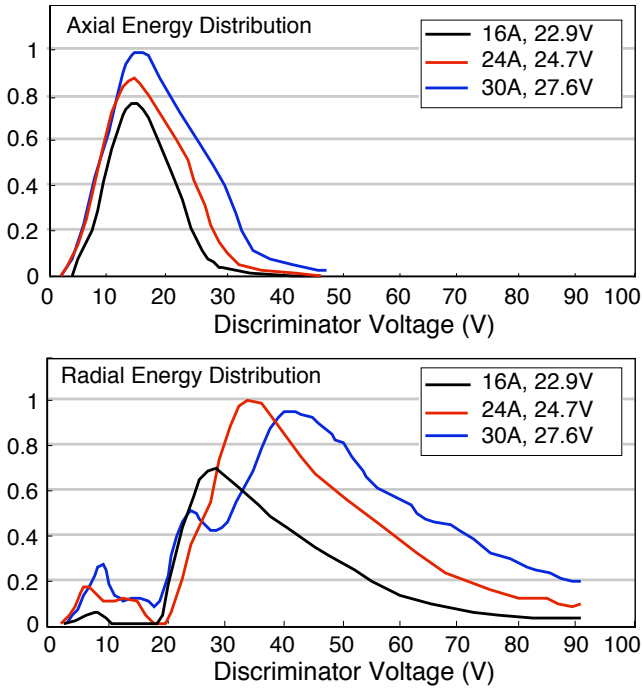


Figure 19. Axially oriented (a) and radially oriented (b) RPA data.

were detected, but were found to be very small in amplitude ($\Delta n/n \approx 1\%$). There were no significant oscillations detected inside the hollow cathode or in the cathode orifice region.

However, when the probes were scanned into the bright “plasma ball” characteristically observed outside the cathode and keeper regions, strong density and potential oscillations were again detected as with the NSTAR cathode. Figure 20a shows the fluctuations in the ion saturation current measured by the transversely scanning probe inserted into the edge of the plasma ball for the nominal 25 A, 5.5 sccm case. The oscillations are relatively incoherent with frequencies of 0.5 to 2 MHz and amplitudes up to 100 percent of the ion saturation current.

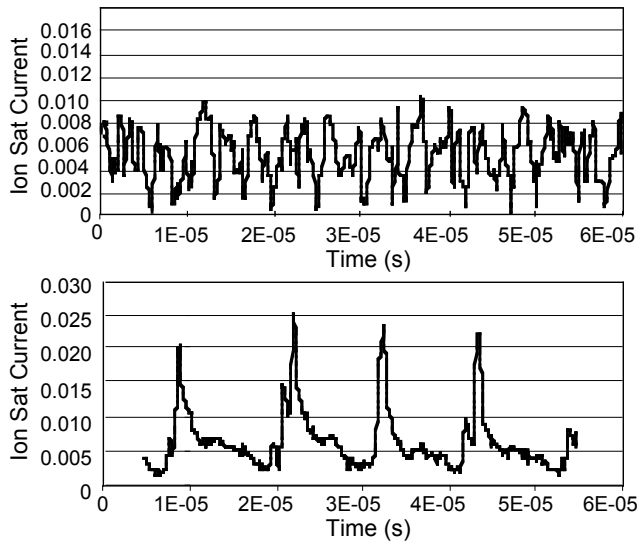


Figure 20. Ion saturation oscillations at edge of plasma ball for 25 A discharge current at 5.5 sccm (a) and 4 sccm (b).

potential hill keeper exit, such as proposed in Ref. 13, at or near the cathode orifice that could produce the energetic ions observed by the radial RPA. The axial RPA data is consistent with ions generated downstream of the gradual potential peak that exists several cm downstream of the cathode and falling into the analyzer, while the radial RPA data cannot be explained by these potential profiles.

It has also been proposed² that plasma instabilities in the double layer inside the cathode orifice can accelerate ions to high energy. Recent theoretical modeling¹⁴ of the plasma region inside the cathode suggested that turbulence near the orifice entrance may develop as a result of wave growth from streaming electrons and ions, which are subject to reduced Landau damping due to the relatively low ion-to-electron temperature ratio (~ 0.1). However, these calculations only extended up to the orifice entrance where turbulent heating is likely due to the increasing electron current densities entering the orifice. To investigate proposed oscillations in the cathode interior or orifice region, the scanning probes were biased to ion saturation and connected to a 1-Gbs digital oscilloscope. Inside the cathode orifice, ion-acoustic type oscillations on the order of 1 MHz

Reducing the gas flow rate, as shown in Fig. 20b, caused the oscillations to change into ≈ 100 kHz large-amplitude spikes characteristic of what we call “predator-prey” oscillations¹⁹. These oscillations are related to an ionization instability caused by burning up the gas locally in the cathode plume. Transition of the oscillations from the high frequency incoherent fluctuations to the low frequency “predator-prey” oscillations could also be achieved by lowering the magnetic field at the cathode exit. The oscillations were observed to increase in frequency and amplitude as the discharge current increased, as shown in Figure 21, or the gas flow decreased. The oscillations appear to be precursors to larger amplitude “plume-mode” oscillations that appear in the discharge voltage and keeper potential at similar frequencies. The transition from incoherent fluctuations to predator-prey type oscillations depends on the discharge current, gas flow rate, and magnetic field, and both types of behavior could be observed over large ranges in the discharge parameters.

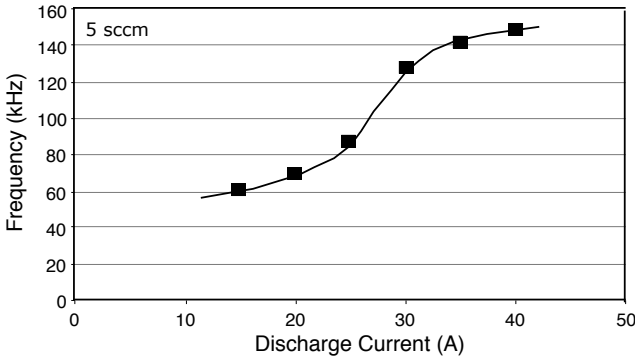


Figure 21. Frequency dependence on discharge current for the low frequency oscillations.

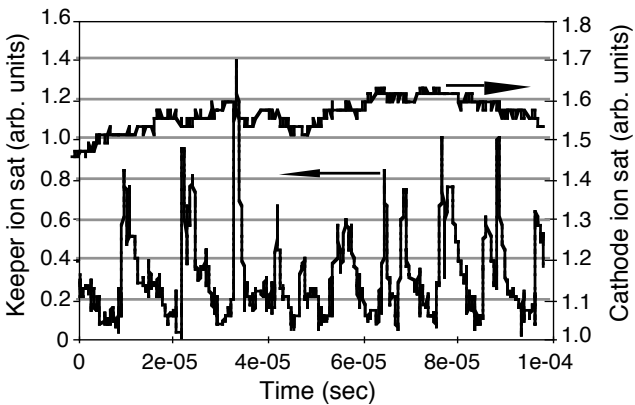


Figure 22. Ion saturation current inside and outside cathode showing now correlation to the oscillations in the hollow cathode insert plasma.

Experiments determined that the oscillations in the plasma ball density did not extend into the interior of the hollow cathode plasma. Figure 22 shows the ion saturation current measured simultaneously by the transverse scanning probe in the plasma ball outside of the cathode and by the axially scanning probe located just upstream of the cathode orifice plate. There is no correlation to the signals, and the fluctuation level inside the hollow cathode is very low.

To further investigate the source of the energetic ions, the transverse scanning probe was again configured as an emissive probe that is operates sufficiently hot to float at the plasma potential²⁰. The high-impedance ($>100 \text{ M}\Omega$) voltage detection circuitry used to measure the DC and rf plasma potential is sensitive to voltage fluctuations of up to 1 MHz at peak voltages of up to 80 V. Figure 23 shows the radial profile of the rf plasma potentials for our nominal case of 25 A at 5.5 xenon flow at two values of the applied magnetic field at the cathode. For the nominal case of 5.5 sccm with 80 G applied, the potential on axis is about 18 V, which is consistent with the scanning Langmuir probe data shown in Fig. 17. With the magnetic field turned down to 10 G, the frequency drops to the predator-prey mode and the amplitude of the oscillations is consistent with the data shown in Fig. 20 on axis. As in NSTAR, the average plasma potential profile forms a well or trough centered on the bright “plasma ball” observed on axis, consistent with the low frequency emissive probe measurements in Ref. 16. The potential

increases radially over several cm to a peak of about 5 V in excess of the discharge voltage that extends to near the anode surface. If the gas flow is decreased as in Fig. 23b, or the magnetic field decreased, the plasma breaks into the large amplitude, 80-kHz oscillations seen in Fig. 20. The rf plasma potential has fluctuations in excess of 60 V in starting at the edge of the ball and extending radially outward to the anode wall.

The ion current collected by the RPA is correlated to the density fluctuations measured by the probes. Figure 24a shows that the high frequency plasma potential oscillations are uncorrelated with the collected RPA current, but the low frequency potential oscillations are inversely correlated ($\approx 180^\circ$ out of phase) with the collected RPA current in Fig. 24b. This is consistent with the ions being born at a high potential near the cathode and flowing to the RPA in bursts at the predator-prey oscillation frequency as the plasma density collapses. Figure 25 shows the transverse Langmuir probe ion current fluctuations measured at the edge of the plasma ball, the RPA collector current and the AC component of the discharge voltage. While the probe and RPA current fluctuations are reasonably well correlated, these fluctuations are not driven by oscillations in the discharge voltage. The discharge voltage oscillations are typically of low frequency ($\leq 1 \text{ kHz}$) consistent with the power supply current regulation time constants.

A direct comparison of the ion energies measured by the radially-positioned RPA for the cases with and without the large amplitude oscillations is shown in Figure 26. We see that the low magnetic field case (with the low frequency oscillations) produces significantly larger numbers of high energy ions compared to the nominal case. It seems very likely that the amplitude of the plasma potential oscillations shown in Fig. 23 are directly related to the number of high energy ions measured in the keeper region in Fig. 26. The mechanisms for accelerating the ions have not been directly determined at this time, but it is likely that any ions born at high potential during an oscillation will fall through the potential drop to the cathode potential RPA and gain that associated energy. This is also true for

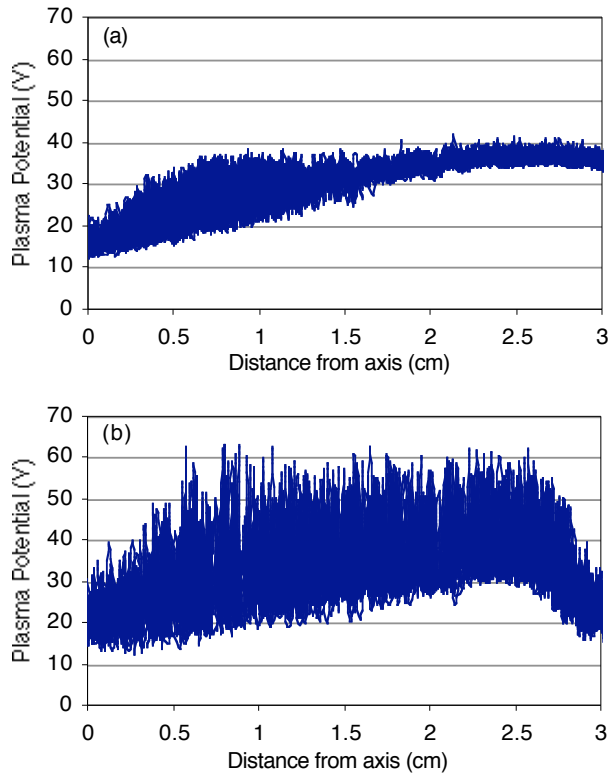


Figure 23. Radial plasma potential profile at 25 A for 5.5 sccm (a) and 4 sccm (b).

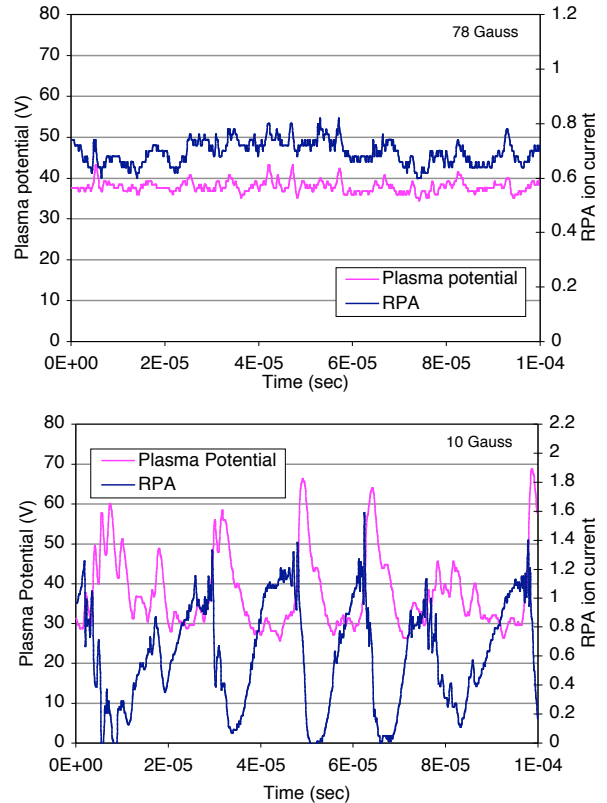


Figure 24. RPA current and plasma potential oscillations for two magnetic fields at 25 A and 5.5 sccm

double ions, which will gain twice the energy falling through the same potential. The fact that high energy ions are also observed (in reduced numbers) with only very high frequency oscillations (0.5-1 MHz) points to additional acceleration mechanisms such as turbulent ion acoustic transport. Theoretical and experimental investigations aimed at understanding the role of the ion acoustic waves in producing the high-energy ions are underway.

Finally, the axial location of the plasma ball in front of the large NEXIS cathode is also observed to change with the discharge parameters. It is generally observed that increases in gas flow, discharge current, and magnetic field all cause the plasma ball to move downstream. Increases in the gas flow generally reduce the observed oscillation level, especially of the low frequency predator-prey modes associated with collapse of the plasma due to burning up

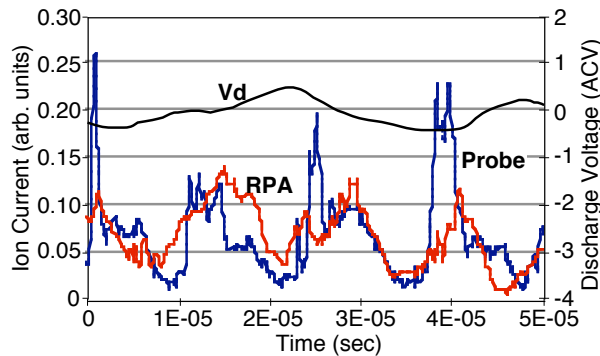


Figure 25. Ion current from scanning probe at the edge of the plasma ball, ion current collected by the RPA, and discharge voltage.

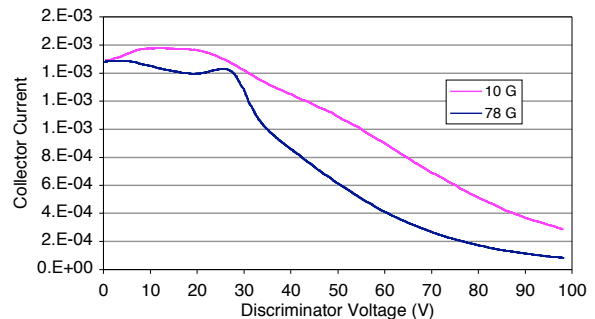


Figure 26. Comparison of RPA current for the case of low magnetic field (low frequency, large amplitude oscillations, and nominal filed)

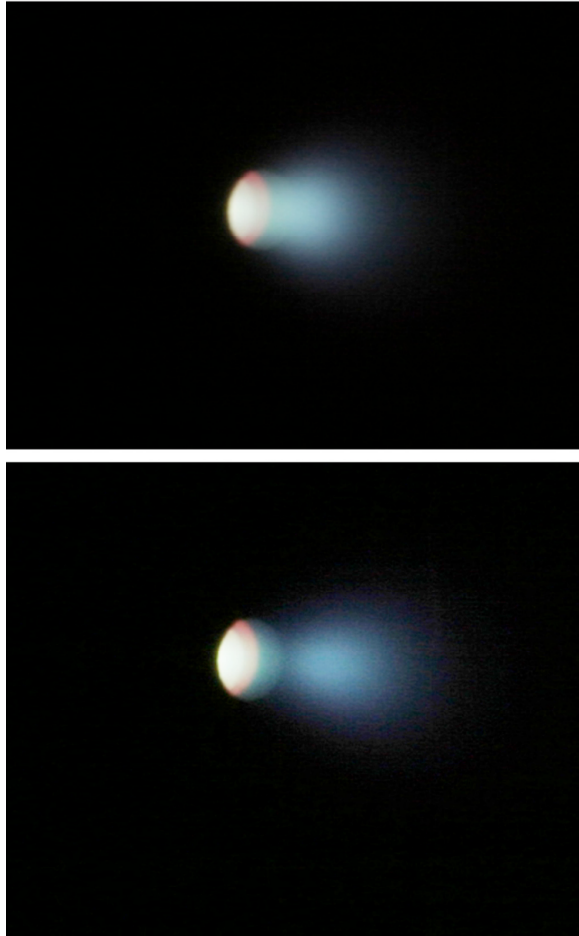


Figure 27. Plasma ball location for the nominal 25A, 5.5 sccm case (top) and a 25 A, 10 sccm case.

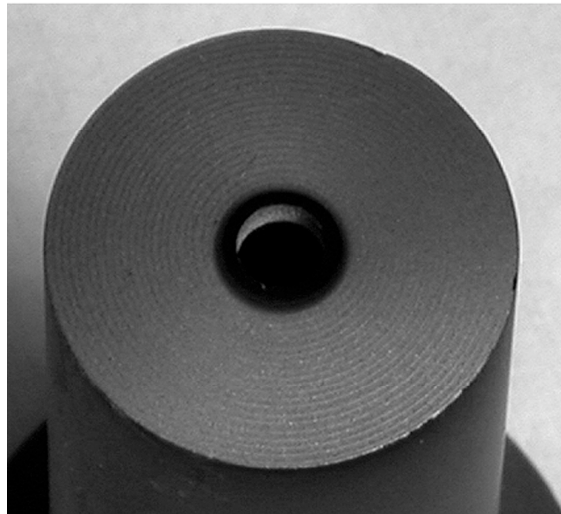


Figure 28. Photo of the NEXIS keeper face after the 2000 hour wear test.

the gas in the cathode plume. Figure 27 shows photographs of the cathode plume for the NEXIS cathode for the nominal 25 A, 5.5 sccm condition (top) and a high flow of 10 sccm case. The plasma ball moved significantly downstream, and a dark space associated with very cold electron temperatures is observed to form between the cathode and the plasma ball. In both cases, the plasma ball is significantly downstream of the keeper orifice. Since the strong oscillations appear related to the plasma ball, it is expected that the NEXIS cathode will have low keeper wear rates. The NEXIS cathode was examined after a recent 2000 hour wear test in the thruster at a nominal current of 27 A and a flow of 6.5 sccm. Careful laser-profilometry measurements indicated that the keeper face and orifice were essentially unchanged from the before-test inspection. Figure 28 is a photograph of the keeper face taken after the test, and shows a uniformly smooth keeper face surface with the exception of some light graphite soot around the orifice. This soot is very weakly bound, and is easily removed by any ion bombardment. The presence of this soot indicates that the keeper orifice region experienced little or no ion bombardment, and so should experience no wear. The smooth surface outside the soot is in contrast to the NSTAR cathode shown in Fig. 7, where the localized ion erosion pattern was evident. This behavior supports the cathode experiments described here that indicate that with the proper cathode/keeper design and with the proper selection of the cathode operating parameters, keeper wear can be mitigated.

V. High Energy Ion Suppression

An attempt was made to suppress the oscillations that lead to the high-energy ions observed in the hollow cathode tests. Since the oscillations appear to be related to either predator-prey modes or turbulent ion acoustic waves, both of which depend strongly on the local gas pressure and plasma temperatures, the keeper electrode was modified to change the geometry and the gas flow pattern at the exit. Figure 29 shows the radial plasma potential profile and oscillations for the NSTAR cathode operating at TH15 and TH8. The large amplitude plasma potential oscillations have been suppressed in both cases. Figure 30 shows the ion energy distribution measured with the radially-positioned RPA for the nominal keeper design, no keeper, and the modified keeper. We see that the keeper modification significantly reduced the high energy ion tail compared to the nominal case. This is consistent with the suppression of the oscillations in Fig. 29.

VI. Conclusion

An investigation of the plasma parameters in the cathode insert, keeper and anode regions of hollow

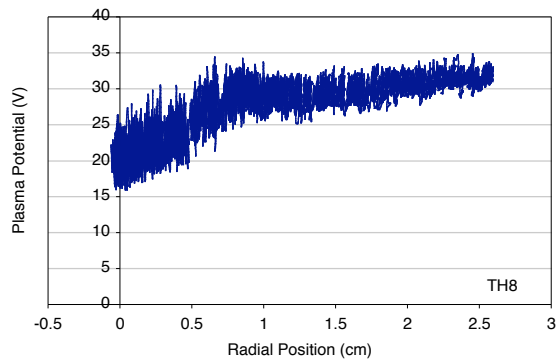
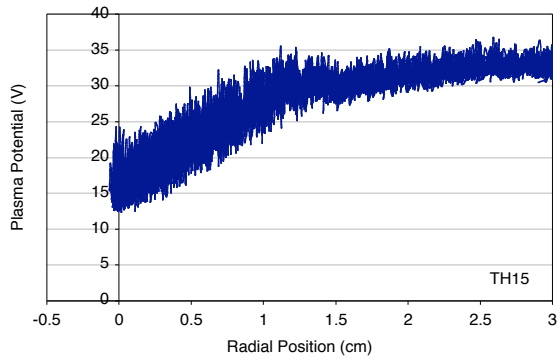


Figure 29. Radial plasma potential oscillations for the NSTAR cathode with the modified keeper at TH15 and TH8 showing oscillation suppression.

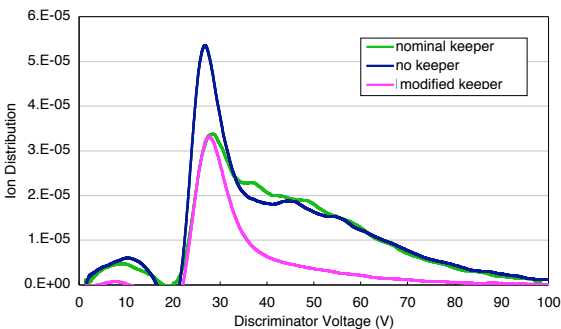


Figure 30. Ion energy distribution for NSTAR TH15 mode operation with the nominal keeper, no keeper, and a modified keeper.

cathodes used in NSTAR and NEXIS ion thrusters has been undertaken to determine the mechanisms high energy ion production and for the keeper erosion. The RPA analyzer showed few high energy ions directed in the downstream axial direction, but a significant number of ions with energies in excess of the discharge voltage and up to 100 eV were found to flow in the radial direction in front of the keeper. The presence of high energy ions in this location that can strike the keeper are consistent with erosion of the keeper face and orifice by sputtering. Detailed measurements of the potential distributions could not find a DC mechanism for acceleration of ions to the high energies (>50 V) observed in these discharges under certain conditions. However, rf measurement of the plasma potential profile show fluctuations in the range of 50-500 kHz exist in the keeper region, with the largest amplitudes occurring at the edge of the plasma ball downstream of the cathode orifice in the keeper region. These oscillations range from ionization instabilities to turbulent ion acoustic waves, and the corresponding current of the high-energy ions collected by the RPA is consistent with the rf ion current and potential fluctuation. The results shown here indicate that proper cathode/keeper design and proper selection of the cathode operating parameters, the plasma oscillations and high ion energies can be suppressed, and the keeper wear can be mitigated.

Acknowledgments

The research described in this paper was carried out by the Jet Propulsion Laboratory, California Institute of Technology, under a contract with the National Aeronautics and Space Administration in support of Project Prometheus.

References

A.T. Forrester, *Large Ion Beams*, Wiley-Interscience, NY, 1988.

V.J. Friedly and P.J. Wilbur, *J. Propulsion and Power*, **8**, 635 (1992).

I. Kameyama and P. Wilbur, *J. Propulsion and Power*, **16**, 529 (2000).

G. Williams, et al., *IEEE T-PS*, **28**, 1664 (2000).

J. Foster and M. Patterson, *J. Propulsion and Power*, **21**, 144 (2005).

M. Croften and I. Boyd, *AIAA Paper 2002-4103*, July 2002.

J.R. Brophy and C.E. Gardner, *AIAA Paper 88-2913*, July 1988.

M. Domonkos, J. Foster, G. Soulas, *J. Propulsion and Power*, **21**, 102 (2005).

J. Polk, et al., *AIAA Paper 97-3387*, July 1997.

A. Sengupta, et al., *AIAA Paper 2004-3608*, July 2004.

J.R. Brophy, *Rev. Sci. Instrum.* **73**, 1071 (2002).

M. Patterson, T. Haag, S. Hovan, *IEPC Paper 93-108*, Sept. 1993.

I. Kameyama, P. Wilbur, *ISTS Paper #98-a-2-17*, 21st Intl. Symp. Space Tech. Sci., Sonic City, Omiya, Japan, May 24-21, 1998.

I. Mikellides, et al., *AIAA Paper 04-3817*, July 2004.

D.M. Goebel, K. Jameson, R. Watkins, I. Katz, AIAA Paper 2004-3430, July, 2004.
D. Herman and A. Gallimore, AIAA Paper 2004-3958, July 2004.
C. Farnell and J. Williams, AIAA Paper 2004-3432, July 2004.
Chen, F. in *Plasma Diagnostics Techniques*, Academic Press, NY, p.113-200 (1966).
Boeuf, J. P. and Garrigues, L., J. of Appl. Phys., Vol. 84, 3541-3554, 1998.
N.Hershkowitz and M Cho, J. Vac.Sci Tech. **A**, 2054 (1988).